and $n = 1$, $K = 10^{6.6}$ (in 0.01 M NaAc), respectively. Because the range for the extent of binding r is limited ($0.7 < r < 1.0$) for this strong binding polymer, the agreement between the calculated curves and the data points in these plots does not support the validity of the independent-site model, however.

One way to circumvent this difficulty was to increase the ionic strength of the medium to 0.05 M NaCl and hence to weaken the binding so that the data points can cover the whole range of r. These data were indeed obtained and analyzed in the same manner as those above for MPVI + MO and are summarized in Table IV. Direct comparison of the parameters K_0 and ω for the two polymer listed in this table is not appropriate because the two systems were not measured at the same ionic strength. Note that the cooperative model seems to describe well both systems when the polymer sites are approximately 70% occupied (i.e., $r = 0.6$–0.7).

Conclusions

1. The 1:1 stoichiometry for complexes of methyl orange and the quaternized poly(*N*-vinylimidazole) homopolymers suggests that binding capacity is dictated primarily by charge.

2. The binding strength between methyl orange and the quaternized polymers is influenced by (a) Coulombic interaction between the anionic dye and polycations, (b) nonionic interaction between the quaternizing side chain and the dye, and (c) nonionic bound dye–dye interaction.

3. The binding behavior in the saturation range $0 < r < 0.7$ can be described by the McGhee–von Hippel expression. The bound dye–dye interaction is associated with the aggregation tendency of the dye, which contributes an additional force to the overall polymer–dye interaction. The cooperative binding cannot persist, however, at a higher saturation level, possibly because of the steric hindrance of the two neighboring dye molecules.

Acknowledgment. We are grateful to Mrs. A. R. Sochor for technical assistance, Dr. I. S. Ponticello and Mr. K. R. Hollister for the preparation of some of the polymers used in this study, and Dr. H. Yu and Dr. J. L. Lippert for discussions during this study.

References and Notes

(1) Frank, H. S.; Evans, M. W. *J. Chem. Phys.* **1945**, *13*, 507.
(2) Kauzmann, W. *Adv. Protein Chem.* **1959**, *14*, 1.
(3) Franks, F. "Water, A Comprehensive Treatise"; Franks, F., Ed.; Plenum Press: New York, 1975; Vol. 4, p 1.
(4) Klotz, I. M.; Royer, G. P.; Sloniewsky, A. R. *Biochemistry* **1969**, *8*, 4752.
(5) Quadrifoglio, F.; Crescenzi, V. *J. Colloid Interface Sci.* **1971**, *35*, 447.
(6) Reeves, R. L.; Harkaway, S. A. "Micellization, Solubilization, and Microemulsions"; Mittal, K. L., Ed.; Plenum Press: New York, 1977; Vol. 2, p 819.
(7) Takagishi, T.; Nakata, Y.; Kuroki, N. *J. Polym. Sci.* **1974**, *12*, 807.
(8) Ando, Y.; Komiyama, J.; Iijima, T. *J. Chem. Soc. Jpn.* **1981**, *3*, 432.
(9) Tan, J. S.; Handel, T. M., to be submitted for publication.
(10) Orchard, B. J.; Tan. J. S.; Hopfinger, A. J. *Macromolecules* **1984**, *17*, 169.
(11) Tan, J. S.; Sochor, A. R. *Macromolecules* **1981**, *14*, 1700.
(12) Tan, J. S.; Gasper, S. P. *J. Polym. Sci. Polym. Phys. Ed.* **1974**, *12*, 1785.
(13) Scholtan, W. *Makromol. Chem.* **1953**, *11*, 131.
(14) Klotz, I. M. "The Proteins, Chemistry, Biological Activity, and Methods"; Neurath, H., Bailey, K., Eds.; Academic Press: New York, 1953; Vol. 1, p 727.
(15) Scatchard, G. *Ann. N.Y. Acad. Sci.* **1949**, *51*, 660.
(16) Tanford, C. "Physical Chemistry of Macromolecules"; Wiley: New York, 1967.
(17) von Hippel, P. H.; Schleich, T. *Acc. Chem. Res.* **1969**, *2*, 257.
(18) Cantor, C. R.; Schimmel, P. R. "Biophysical Chemistry"; W. H. Freeman: San Francisco, 1980; Part III.
(19) McGhee, J. D.; von Hippel, P. H. *J. Mol. Biol.* **1974**, *86*, 469.
(20) Schwarz, G. *Eur. J. Biochem.* **1970**, *12*, 442.
(21) Crothers, D. M. *Biopolymers* **1968**, *6*, 575.
(22) Hill, A. V. *J. Physiol. (London)* **1910**, *40*, iv.
(23) Coates, E. *J. Soc. Dyers Colour.* **1969**, *85*, 355.
(24) Hewitt, M.; Handel, T. M.; Tan, J. S., unpublished data.

Shape of Unperturbed Linear Polymers: Polypropylene

Doros N. Theodorou and Ulrich W. Suter*

Department of Chemical Engineering, Massachusetts Institute of Technology, Cambridge, Massachusetts 02139. *Received July 30, 1984*

ABSTRACT: Large numbers of conformations of unperturbed polypropylene chains are generated in Monte Carlo experiments, based on a rotational isomeric state scheme, and the average instantaneous shape in the system of principal axes of gyration is evaluated. Several new shape measures are introduced to characterize the shape anisotropy, asphericity, and acylindricity. Significant differences are found between short- and medium-length chains of different tacticity, while for long chains all shape measures converge to a common limit. The detailed three-dimensional segment density distributions are examined, and they are found to be bimodal along the longest principal axis of gyration. The loci of highest segment density are always two clearly separated domains, not containing the center of gyration, and they lie on the major principal axis separated by ca. $1.3\langle s^2\rangle_0^{1/2}$–$2.0\langle s^2\rangle_0^{1/2}$. The core of the segment distribution of an unperturbed chain is therefore dumbbell-like in shape.

Introduction

Flexible-chain molecules can assume a large number of conformations and shapes due to the many internal degrees of freedom. The *average shape* of these molecules is of importance for a variety of phenomena, especially for dilute-solution hydrodynamics. Commonly the segment distribution for long chains around their center of mass is examined as an average over all possible orientations in space, i.e., integrating over the external degrees of freedom, and spherical distributions of approximately Gaussian shape are obtained.[1-4] As early as 1934, however, Kuhn had realized[5] that the *instantaneous shape* of polymer coils, observed without orientational averaging, is far from spherical. Average shapes obtained without orientational averaging are therefore necessarily aspherical, and the accurate characterization of these shapes is relevant for the interpretation of phenomena with characteristic time scale smaller than the largest relaxation time of the

0024-9297/85/2218-1206$01.50/0

Table I
Eigenvalues of the Average Instantaneous Radius of Gyration Tensor for Simple Linear Chain Models

type of chain		$\langle\overline{X^2}\rangle/nl^2$	$\langle\overline{Y^2}\rangle/nl^2$	$\langle\overline{Z^2}\rangle/nl^2$	$\langle\overline{X^2}\rangle/\langle\overline{Z^2}\rangle$	$\langle\overline{Y^2}\rangle/\langle\overline{Z^2}\rangle$	ref
random walk on a simple cubic lattice	$n = 50$	0.1270	0.029 06	0.010 75	11.8	2.7	8, 9
	$n = 100$	0.1256	0.029 16	0.010 77	11.7	2.7	8, 9
approximate analytical solution for freely jointed chain	$n \to \infty$	0.125	0.029 8	0.011 8	10.6	2.5	10
Monte Carlo estimation with the rotational isomeric state model of polyethylene	$n = 1000$				12.0	2.7	6

molecule.[6] Even in situations of long-time scale, however, the shape of the individual chains can play an important role; in viscous flow, Zimm[26] showed, orientational preaveraging of chain conformations may lead to significant error, and consideration of the chains as an ensemble of rigidly translating and rotating bodies is a much better approximation. Considerable work has been done in exploring size and shape characteristics; an excellent review of the literature prior to 1977 was written by Šolc.[7]

Šolc and Stockmayer[8,9] were the first to explicitly address the shape of flexible polymer chains; they introduced as shape measure the eigenvalues of the radius of gyration tensor, $\overline{X^2}$, $\overline{Y^2}$, and $\overline{Z^2}$, and presented on elegant analytical method for the evaluation of the symmetric sums of the average moments of the form

$$\sum_{\text{all permutations of } u,\, v,\, w} \langle \overline{X}^{2u}\overline{Y}^{2v}\overline{Z}^{2w}\rangle$$

where the angle brackets denote an average over all conformations. The individual principal components could only be estimated by numerical techniques, however. An approximate analytical method was introduced by Koyama,[10] yielding essentially the same values for $\langle\overline{X^2}\rangle$, $\langle\overline{Y^2}\rangle$, and $\langle\overline{Z^2}\rangle$ as the random-walk results of Šolc and Stockmayer.[8,9] Yoon and Flory[6] were the first to estimate these quantities for a realistic chain model, the rotational isomeric state model of polyethylene, and they obtained values in excellent agreement with the previously reported results for long linear chains. Results for the eigenvalues of the average instantaneous radius of gyration tensor, obtained by these different authors, are shown in Table I. More recently Mattice has obtained values for $\langle\overline{X^2}\rangle$, $\langle\overline{Y^2}\rangle$, and $\langle\overline{Z^2}\rangle$ by Monte Carlo calculations with rotational isomeric models for triglycerides,[11] lecithins,[12] poly(oxyethylene),[13] some polypeptides,[14] and bolaform electrolytes.[15] All these results concern only unperturbed linear chains; there have been several puplications dealing with the effect of solvent quality on the size and form of the radius of gyration tensor, as well as with branched and cyclic polymers, but we limit the scope of this paper to unperturbed linear chains only.

The specification of the three eigenvalues of the radius of gyration tensor naturally leads to the image of an ellipsoidal shape, $\langle\overline{X^2}\rangle$, $\langle\overline{Y^2}\rangle$, and $\langle\overline{Z^2}\rangle$ being the semiaxes of the ellipsoid. The limitations of this picture can only be avoided by evaluation of more detailed information on the spatial segment density distribution. Rubin and Mazur[16] were the first to investigate the detailed three-dimensional density distribution in the principal axis system; for unrestricted and self-avoiding random walks they plotted histograms, projected along the three principal axes of the radius of gyration tensor, which demonstrate clearly that the segment distribution along the "longest" axis is much flatter than those along the two "shorter" axes. We follow this line of investigation with the analysis of the three-dimensional density distribution of an unperturbed vinyl polymer, polypropylene. Investigation of the effects of chain length and tacticity will allow us to identify features general to all chains as well as structure-dependent variations.

Measures of Shape

Consider a chain with n skeletal bonds, numbered from 1 to n, and $n + 1$ skeletal atoms, numbered from 0 to n, in a particular conformation. The center of gravity of the chain is defined so that $\sum_{i=0}^{n}\mathbf{s}_i = \mathbf{0}$, where $\mathbf{s}_i = \text{col}\,(x_i,y_i,z_i)$ is the position vector of skeletal atom i in a frame of reference with origin at the center of gravity. We form the dyadic $\mathbf{s}_i\mathbf{s}_i^{\mathrm{T}}$ and consider its average value over all skeletal atoms, the *radius of gyration tensor*

$$\mathbf{S} = \frac{1}{n+1}\sum_{i=0}^{n}\mathbf{s}_i\mathbf{s}_i^{\mathrm{T}} = \overline{\mathbf{s}\mathbf{s}^{\mathrm{T}}} = \begin{bmatrix} \overline{x^2} & \overline{xy} & \overline{xz} \\ \overline{xy} & \overline{y^2} & \overline{yz} \\ \overline{xz} & \overline{yz} & \overline{z^2} \end{bmatrix} \tag{1}$$

where the overbar denotes averaging over all backbone atoms in the chain. Transformation to a *principal axis system* diagonalizes $\mathbf{S}$, and we choose that principal axis system in which

$$\mathbf{S} = \text{diag}\,(\overline{X^2},\overline{Y^2},\overline{Z^2}) \tag{2}$$

so that the eigenvalues of $\mathbf{S}$, $\overline{X^2}$, $\overline{Y^2}$, and $\overline{Z^2}$, are in descending order, i.e., $\overline{X^2} \geq \overline{Y^2} \geq \overline{Z^2}$. The first invariant[17] of $\mathbf{S}$ is the squared *radius of gyration*

$$s^2 = I_1 = \text{tr}\,(\mathbf{S}) = \overline{X^2} + \overline{Y^2} + \overline{Z^2} \tag{3}$$

a measure of the average size of the particular conformation. Chains consisting of segments of equal mass have by definition[18] a *moment of inertia tensor* (with respect to the center of gravity), $\mathbf{I}$, which is diagonal in the same frame of reference as $\mathbf{S}$ (see Appendix).

The *shape anisotropy* of a chain in a particular conformation shall be defined as the traceless deviatoric part of $\mathbf{S}$

$$\hat{\mathbf{S}} = \mathbf{S} - \tfrac{1}{3}\,\text{tr}\,(\mathbf{S})\mathbf{E} \tag{4}$$

[$\text{tr}\,(\hat{\mathbf{S}}) = 0$] where $\mathbf{E}$ is the unit tensor. In the principal axis system we segment $\hat{\mathbf{S}}$, in a way similar to Smith and Mortensen's treatment of the molecular polarizability tensor,[19] into two terms (each consisting of a scalar and a constant numerical tensor)

$$\hat{\mathbf{S}} = b\,\text{diag}\,(\tfrac{2}{3}, -\tfrac{1}{3}, -\tfrac{1}{3}) + c\,\text{diag}\,(0, \tfrac{1}{2}, -\tfrac{1}{2}) \tag{5}$$

Thus, we define the *asphericity* b

$$b = \overline{X^2} - \tfrac{1}{2}(\overline{Y^2} + \overline{Z^2}), \qquad b \geq 0 \tag{6}$$

and the *acylindricity* c

$$c = \overline{Y^2} - \overline{Z^2}, \qquad c \geq 0 \tag{7}$$

The quantities b and c are useful in characterization of shape; for shapes of tetrahedral or higher symmetry $b = c = 0$, and for shapes of cylindrical symmetry $c = 0$.

An overall measure of shape anisotropy is the quantity $\text{tr}\,(\hat{\mathbf{S}}\hat{\mathbf{S}})$, a simple function of the invariants of $\mathbf{S}$[17]

$$\text{tr}\,(\hat{\mathbf{S}}\hat{\mathbf{S}}) = \tfrac{2}{3}b^2 + \tfrac{1}{2}c^2 = \tfrac{2}{3}I_1^2 - 2I_2 \tag{8}$$

and we use it to define the dimensionless *relative shape anisotropy* κ^2 as

$$\kappa^2 = \frac{3}{2}\,\mathrm{tr}\,(\hat{\mathbf{S}}\hat{\mathbf{S}})/\{\mathrm{tr}\,(\mathbf{S})\}^2 = (b^2 + \frac{3}{4}c^2)/s^4 \qquad (9)$$

which is also a simple function of the invariants of $\mathbf{S}$[17]

$$\kappa^2 = 1 - 3I_2/I_1^2 \qquad (10)$$

The relative shape anisotropy can assume values between 0 and 1 (note that $\overline{X^2} \geq \overline{Y^2} \geq \overline{Z^2}$). A linear array of skeletal atoms (i.e., a rigid-rod molecule), for example, is characterized by $\kappa^2 = 1$; for a regular planar array such as masses at the vertices of a regular polygon or a homogeneously filled polygon $\kappa^2 = {}^1/_4$; for structures of tetrahedral or higher symmetry, $\kappa^2 = 0$.

Up to now only a single-chain conformation has been considered. The average shape of a chain molecule is reflected in the statistical mechanical averages of the measures introduced above, over all possible conformations of the chain, each taken in its principal axis system. These ensemble averages will be denoted by angular brackets; i.e., $\langle a \rangle$ is the conformation average of a. Some of these quantities can be obtained by exact matrix methods if a rotational isomeric state scheme is employed: the average square radius of gyration $\langle s^2 \rangle_0$ and the average square end-to-end distance $\langle r^2 \rangle_0$ (and hence the characteristic ratio $C_n = \langle r^2 \rangle_0 / nl^2$) were computed by standard matrix methods[20] (the subscript zero denotes averages over ensembles unperturbed by the effects of excluded volume).

The shape measures $\langle b \rangle_0$, $\langle c \rangle_0$, $\langle \mathrm{tr}\,(\hat{\mathbf{S}}\hat{\mathbf{S}}) \rangle_0$, and the average relative shape anisotropy

$$\langle \kappa^2 \rangle_0 = 1 - 3\langle I_2/I_1^2 \rangle_0 = \frac{3}{2}\langle \mathrm{tr}\,(\hat{\mathbf{S}}\hat{\mathbf{S}})/\{\mathrm{tr}\,(\mathbf{S})\}^2 \rangle_0 \qquad (11)$$

however, cannot be evaluated exactly; for their estimation Monte Carlo methods were used.

Molecular Model

Polypropylene, represented by the molecular formula CH_3–$[CH(CH_3)CH_2]_x$–H, is a vinyl polymer with well-established conformational characteristics and a fully defined rotational isomeric state scheme.[21] Three tacticities were examined, characterized by Bernoullian diad distributions with meso-diad probability w_m: syndioactic chains (w_m = 0), atactic chains (w_m = 0.5), and isotactic chains (w_m = 1). All parameters were taken from Suter and Flory's work[21] for a temperature of 298 K. Chains of degree of polymerization $x = 5$ to $x = 999$, i.e., with 10–1998 skeletal C–C bonds, were employed.

Monte Carlo "Experiments"

A computer experiment consisted in generating an ensemble of chains of specified tacticity (w_m) and length ($n = 2x$) in order to estimate the quantities of interest. A chain of defined tacticity was generated as a Bernoullian sequence of diads, and a conformation was selected at random by recourse to an "equivalent Markov" scheme:[22] the a priori probabilities for bond 2 to be in state ξ, $p_{\xi;2}$, and the conditional probabilities for all bonds $3 \leq i \leq n - 1$ to be in state ξ given that bond $i - 1$ is in state ζ, $p_{\zeta\xi;i}$, were obtained by appropriate multiplication of statistical weight matrices, and a conformation selected by Monte Carlo simulation.

Each chain is translated from its original frame of reference (i.e., that of bond 1) so that its center of gravity coincides with the new origin. The radius of gyration tensor $\mathbf{S}$ is then obtained according to eq 1 and the three invariants I_1, I_2, and I_3[17] are computed. $\mathbf{S}$ is analytically diagonalized by solution of the cubic secular equation $\lambda^3 - I_1\lambda^2 + I_2\lambda - I_3 = 0$ for the three eigenvalues λ_1, λ_2, and λ_3, which are sorted and identified with $\overline{X^2}$, $\overline{Y^2}$, and $\overline{Z^2}$. s^2, b, c, tr $(\hat{\mathbf{S}}\hat{\mathbf{S}})$, and κ^2 are then computed. The eigenvectors corresponding to $\overline{X^2}$, $\overline{Y^2}$, and $\overline{Z^2}$ are subsequently calculated and the coordinates of all skeletal carbon atoms are transformed to the principal axis system by using the eigenvector matrix as transformation matrix between $\mathbf{S}$ in the original frame of reference and the chosen principal axis system.

Table II
Sample Sizes Used in the Monte Carlo Experiments

	N^b		
x^a	$w_m = 0$	$w_m = 0.5$	$w_m = 1$
5	5000	5000	5000
7	20000	20000	20000
8	15000		
9	15000	15000	15000
10	15000		
11	5000	5000	5000
12	10000		
13	10000		
21	3000	2000	2000
41	2000	1000	5000
61	1500	750	500
81	1000	500	500
101	500	500	500
151		500	
201	500	500	200
301	500	500	500
401		500	
501	500	500	500
751	300	200	200
999	150	100	150

[a] Degree of polymerization. [b] Number of chains.

In order to obtain information on the detailed distribution of the segment cloud in the principal axis system a cube centered at the center of gravity and with edges parallel to the principal axes is subdivided into a grid of $40 \times 40 \times 40$ cells (the dimensions of the cube are chosen large enough that all chains in a given ensemble fit into its boundaries, and small enough to provide adequate resolution; typically an edge length of $2\langle r^2 \rangle_0^{1/2}$ was used). The number of skeletal carbon atoms found in each cell is then counted, giving the distribution of segments for this conformation.

During a computer experiment these processes are repeated a number of times and the average values and standard deviations of all quantities computed are accumulated. At the end of an experiment the segment distribution is "symmetrized" by averaging the cell contents over all octants around the center of the cube. A rather well-resolved distribution of the segment density $\rho(x,y,z)$ in space is thus obtained. The number of chains, N, generated for each ensemble of given tacticity and chain length is listed in Table II.

Results and Discussion

The mean-square end-to-end distances $\langle r^2 \rangle_0$, the mean-square radii of gyration $\langle s^2 \rangle_0$, and the radius of gyration tensors $\langle \mathbf{S} \rangle_0$ (computed in the frame of reference of the first bond of the chains) were estimated for all ensembles in Table II and compared to the corresponding values obtained by exact matrix multiplication[6,20,23] in order to check the simulations; agreement was excellent. This estimate of $\langle \mathbf{S} \rangle_0$ rapidly approached, of course,[7] with increasing chain length a scalar tensor of spherical shape. It was observed that the ratio $\langle r^2 \rangle_0 / \langle s^2 \rangle_0$, being ca. 8 ± 1 for $x = 5$, decreased rapidly to its "Gaussian" value, 6, with increasing chain length, and on the basis of this measure a chain of 300 bonds is essentially Gaussian.

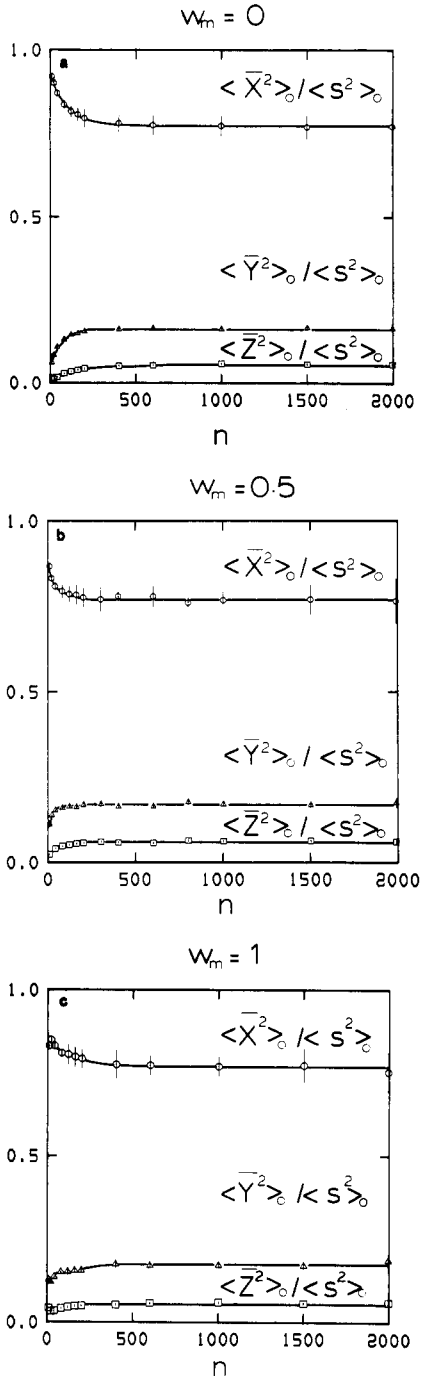

Figure 1. (a) Three eigenvalues of the average instantaneous radius of gyration tensor, divided by the mean-square radii of gyration, vs. chain length ($n = 2x$) for syndiotactic polypropylene. Vertical bars denote standard deviations of the mean values. (b) Same as Figure 1a, but for atactic polypropylene with 50% meso diads. (c) Same as Figure 1a, but for isotactic polypropylene.

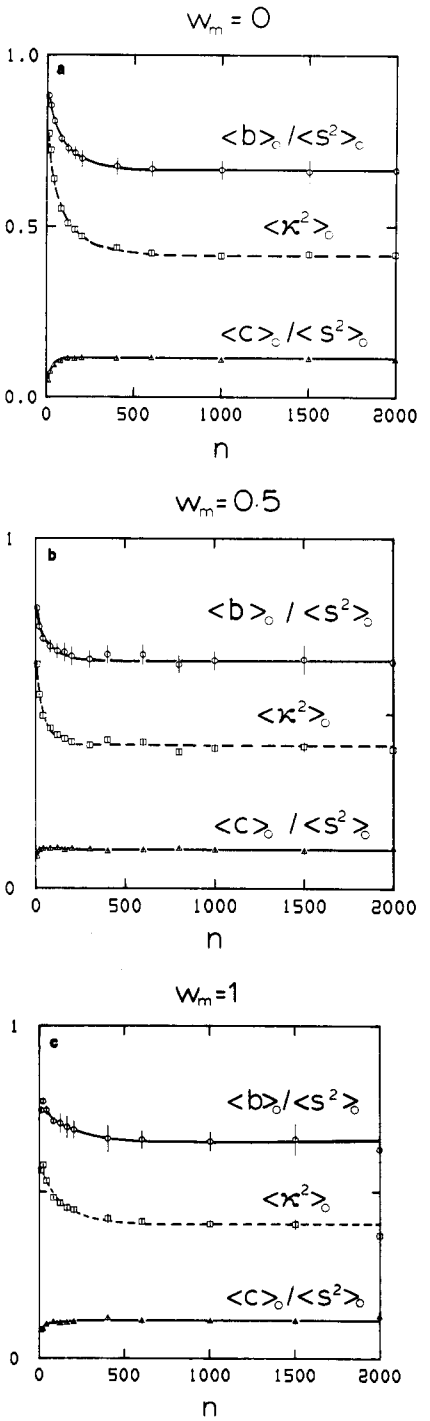

Figure 2. (a) The average asphericity, $\langle b \rangle_0$, and the average acylindricity, $\langle c \rangle_0$, both divided by the mean-square radius of gyration, vs. chain length ($n = 2x$) for syndiotactic polypropylene. The dashed line represents the average relative anisotropy coefficient, $\langle \kappa^2 \rangle_0$. Vertical bars denote standard deviations of the mean values. (b) Same as Figure 2a, but for atactic polypropylene with 50% meso diads. (c) Same as Figure 2a, but for isotactic polypropylene.

The quantities characterizing shape, on the other hand, never approached the values expected for a spherical distribution of segments. The average eigenvalues $\langle \overline{X^2} \rangle_0$, $\langle \overline{Y^2} \rangle_0$, and $\langle \overline{Z^2} \rangle_0$ (eq 2), after division by $\langle s^2 \rangle_0$, are plotted in Figure 1 for the three tacticities examined. In all cases $\langle \overline{X^2} \rangle$ decreases, and $\langle \overline{Y^2} \rangle$ and $\langle \overline{Z^2} \rangle$ increase with increasing chain length, but at $n = 500$ the reduced principal axes have settled to their limiting values. The values at $x = 999$ are reported in Table III; they are indistinguishable among the three tacticities and compare well with Koyama's[10] approximate analytical values for infinite (Gaussian) chains: $\langle \overline{X^2} \rangle_0 / \langle s^2 \rangle_0 = 0.754$, $\langle \overline{Y^2} \rangle_0 / \langle s^2 \rangle_0 = 0.175$, $\langle \overline{Z^2} \rangle_0 / \langle s^2 \rangle_0 = 0.0646$. Note that in Figure 1 the values for atactic chains approach the limits more rapidly than the stereoregular chains; this is a general characteristic, observed with all shape and size measures.

The average asphericities $\langle b \rangle_0$ (eq 6), and the average acylindricities $\langle c \rangle_0$ (eq 7), both divided by $\langle s^2 \rangle_0$, as well as the average relative anisotropy coefficients $\langle \kappa^2 \rangle_0$ (eq 11) are plotted in Figure 2. It is evident that the shortest chains are very cylindrical in shape and that they become somewhat less cylindrical and a little more spherical with increasing chain length; the syndiotactic chains (for which asymptotic limits are only reached at $n \approx 750$) show these

Table III
Limiting Shape Measures for Polypropylene Chains

measure	x	tacticity $w_m = 0$	$w_m = 0.5$	$w_m = 1$
$\langle\overline{X^2}\rangle_0/\langle s^2\rangle_0$	999	0.78 ± 0.05	0.77 ± 0.06	0.75 ± 0.06
$\langle\overline{Y^2}\rangle_0/\langle s^2\rangle_0$	999	0.17 ± 0.01	0.17 ± 0.01	0.19 ± 0.01
$\langle\overline{Z^2}\rangle_0/\langle s^2\rangle_0$	999	0.058 ± 0.003	0.060 ± 0.004	0.060 ± 0.003
$\langle b\rangle_0/\langle s^2\rangle_0$	751	0.66 ± 0.03	0.66 ± 0.04	0.66 ± 0.05
$\langle c\rangle_0/\langle s^2\rangle_0$	751	0.110 ± 0.006	0.106 ± 0.007	0.113 ± 0.008
$\langle\kappa^2\rangle_0$	751	0.42 ± 0.01	0.41 ± 0.01	0.40 ± 0.01
$^3/_2\langle\mathrm{tr}\,(\hat{\mathbf{S}}\hat{\mathbf{S}})\rangle/\langle\mathrm{tr}\,(\mathbf{S})\rangle^2$	999	0.66 ± 0.09		0.69 ± 0.12
$\langle\overline{X^2}\rangle_0/\langle\overline{Z^2}\rangle_0$	999	13.4 ± 0.8	12.7 ± 0.9	12.5 ± 0.8
$\langle\overline{Y^2}\rangle_0/\langle\overline{Z^2}\rangle_0$	999	2.9 ± 0.2	2.9 ± 0.2	3.1 ± 0.2

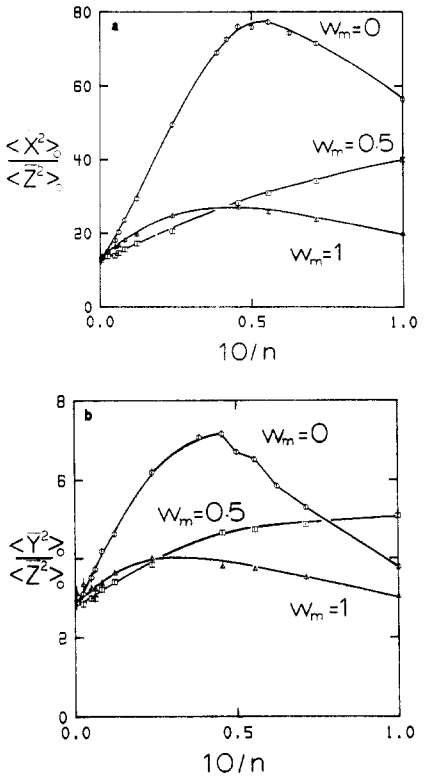

Figure 3. (a) Ratio of the largest to the smallest eigenvalue of the average instantaneous radius of gyration tensor, vs. the inverse chain length ($n = 2x$), for syndiotactic ($w_m = 0$), atactic ($w_m = 0.5$), and isotactic ($w_m = 1$) polypropylene. Vertical bars denote standard deviations of the mean values. (b) Ratio of the two smaller eigenvalues of the average instantaneous radius of gyration tensor, vs. the inverse chain length ($n = 2x$). See Figure 3a.

features in a somewhat more pronounced way than the atactic and isotactic chains (for which the limits are reached at $n \approx 200$). The limiting values of $\langle b\rangle_0/\langle s^2\rangle_0$ and $\langle c\rangle_0/\langle s^2\rangle_0$ are included in Table III; they are indistinguishable among the three tacticities. The average relative shape anisotropy $\langle\kappa^2\rangle_0$ is a decreasing function of chain length in all cases; its dependence on chain length is stronger than that of $\langle b\rangle_0/\langle s^2\rangle_0$ and $\langle c\rangle_0/\langle s^2\rangle_0$, and it converges only at $n \approx 750$. The limiting values are also listed in Table III.

The average ratios required in eq 11, i.e., $\langle I_2/I_1^2\rangle_0$ or $\langle\mathrm{tr}\,(\hat{\mathbf{S}}\hat{\mathbf{S}})/\{\mathrm{tr}\,(\mathbf{S})\}^2\rangle_0$, have not yet yielded to analytical evaluation. Šolc[9] has obtained the individual averages

$$\langle\overline{X^2} + \overline{Y^2} + \overline{Z^2}\rangle_0 \equiv \langle s^2\rangle_0 \equiv \langle I_1\rangle_0 = {}^1/_6(1 - 1/n^2) \quad (12)$$

$$\langle\overline{X^2Y^2} + \overline{Y^2Z^2} + \overline{Z^2X^2}\rangle_0 \equiv \langle I_2\rangle_0 = (1/180)(1 - 5/n^2 + 4/n^4) \quad (13)$$

$$\langle(\overline{X^2})^2 + (\overline{Y^2})^2 + (\overline{Z^2})^2\rangle_0 = (1/540)(13 + 10/n^2 - 23/n^4) \quad (14)$$

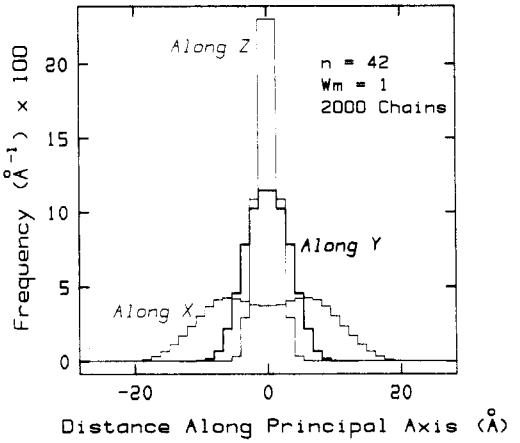

Figure 4. Histograms of the average segment distribution in an isotactic polypropylene of 21 units, projected along the three principal axes of the instantaneous radius of gyration tensor.

for freely jointed chains with Gaussian segments, however. These equations, together with the relationship

$$\frac{{}^3/_2\langle\mathrm{tr}\,(\hat{\mathbf{S}}\hat{\mathbf{S}})\rangle/\langle\mathrm{tr}\,(\mathbf{S})\rangle^2}{} = \frac{\langle(\overline{X^2})^2 + (\overline{Y^2})^2 + (\overline{Z^2})^2\rangle - \langle\overline{X^2Y^2} + \overline{Y^2Z^2} + \overline{Z^2X^2}\rangle}{\langle\overline{X^2} + \overline{Y^2} + \overline{Z^2}\rangle^2} \quad (15)$$

yield an exact limiting value for all infinite chains:

$$\lim_{n\to\infty} \{{}^3/_2\langle\mathrm{tr}\,(\hat{\mathbf{S}}\hat{\mathbf{S}})\rangle_0/\langle\mathrm{tr}\,(\mathbf{S})\rangle_0^2\} = {}^2/_3 \quad (16)$$

The corresponding values from our Monte Carlo experiments are given in Table III; they agree with the exact limit (eq 16), but are plagued by very strong fluctuations. Another limiting ratio corresponding to eq 16 is obtained from eq 12 and 14

$$\lim_{n\to\infty} \{1 - 3\langle I_2\rangle_0/\langle I_1\rangle_0^2\} = {}^2/_5 \quad (17)$$

It is pure coincidence, of course, that this ratio is surprisingly close to the values of $\langle\kappa^2\rangle_0$ reported in Table III.

The data displayed in Figure 2 have been replotted in Figure 3 as ratios of the length of the squared principal axes, $\langle\overline{X^2}\rangle_0/\langle\overline{Z^2}\rangle_0$ and $\langle\overline{Y^2}\rangle_0/\langle\overline{Z^2}\rangle_0$, vs. the inverse chain length. Striking differences are observed among the different tacticities in the region of short chains: the static chains yield a monotonic dependence for each ratio, the isotactic chains show modest maxima around $n \approx 30$, and the syndiotactic chains exhibit more pronounced maxima at $n \approx 20$. The corresponding ratios of eigenvalues for polyethylene computed by Yoon and Flory do not extend to values $n < 20$, but behave, at least qualitatively, similarly to those of the atactic polypropylenes (Figure 3). All tacticities converge to the same limiting values, displayed in Table III. These limits compare fairly well with those listed in Table I.

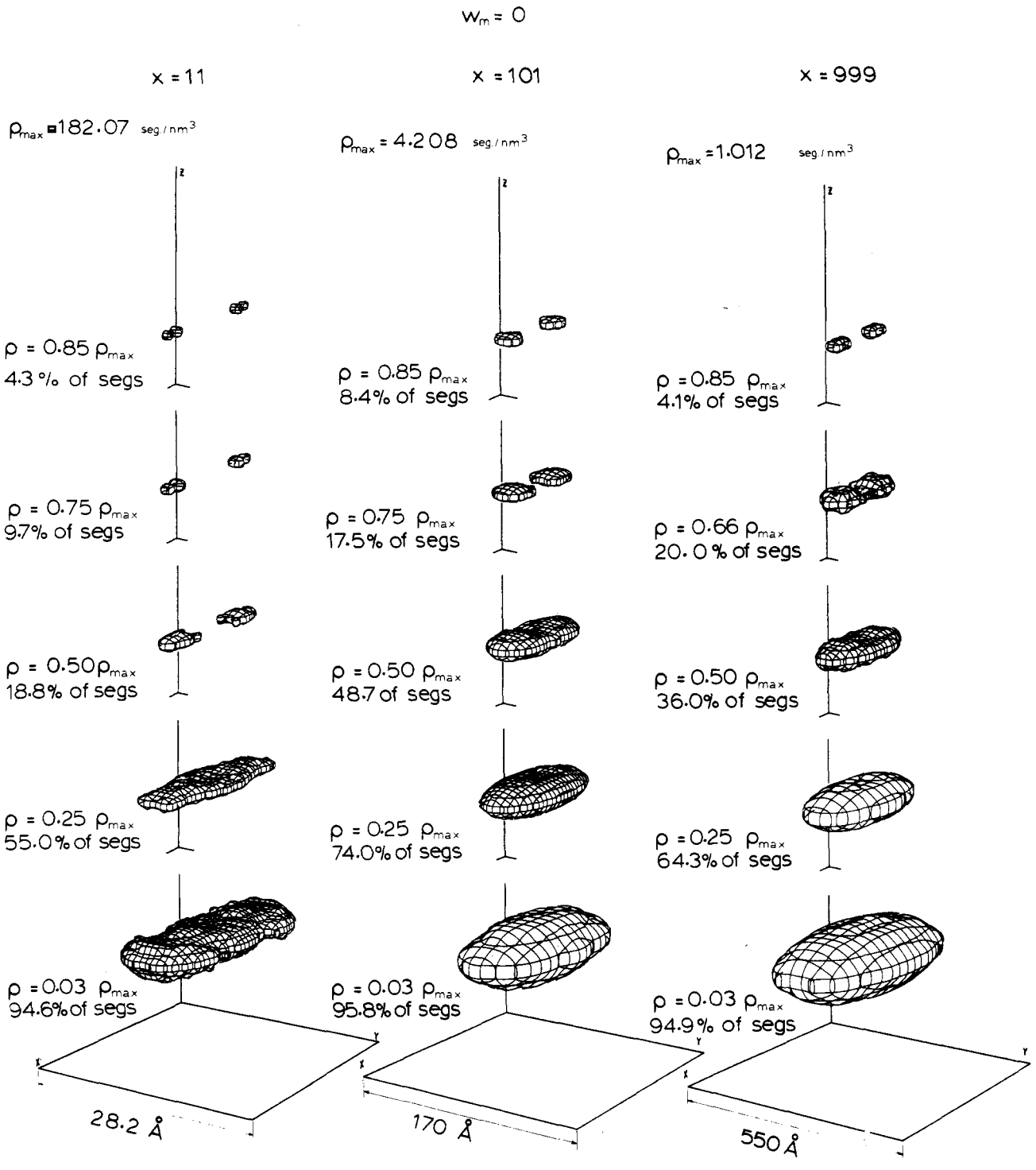

Figure 5. Surfaces of equal average segment density for syndiotactic chains of chain length $x = 11$, $x = 101$, and $x = 999$. Surfaces are drawn at the indicated fractions of the maximum segment density in the domains of the chains. The axes are parallel to the principal axes of the average instantaneous radius of gyration tensor; they are the edges of the 40 × 40 × 40 grid used to construct the surfaces and are all of equal length.

From the combined results, so far, it is evident that different measures of shape are sensitive to a very different degree to chain length and structure (i.e., tacticity).

Rubin and Mazur[16] have plotted histograms of the segment distribution along the three principal axes of their model chains and noted qualitative differences between different projections, especially an unusual "flatness" for those projections along the major principal axis, X. The corresponding projections for isotactic polypropylene of chain length $x = 21$ are shown in Figure 4. Rubin and Mazur's observations are confirmed, but in addition it is obvious that the projected distribution along the X axis is not simply flat, but has a *minimum* at the center. The shape of these projections is essentially the same for all chains, regardless of length or tacticity (only the spread and height of the histograms, and the location of the maxima along the X axis, change). The depth of the central minimum decreases slightly as n increases, but the projection is never actually flat; i.e., the bimodal appearance persists up to the longest chains examined ($x = 999$). This points to a *dumbbell-like character* of the instantaneous shape of unperturbed polymers, i.e., of both real chains at a Θ-state and simple model chains.

The detailed examination of the three-dimensional

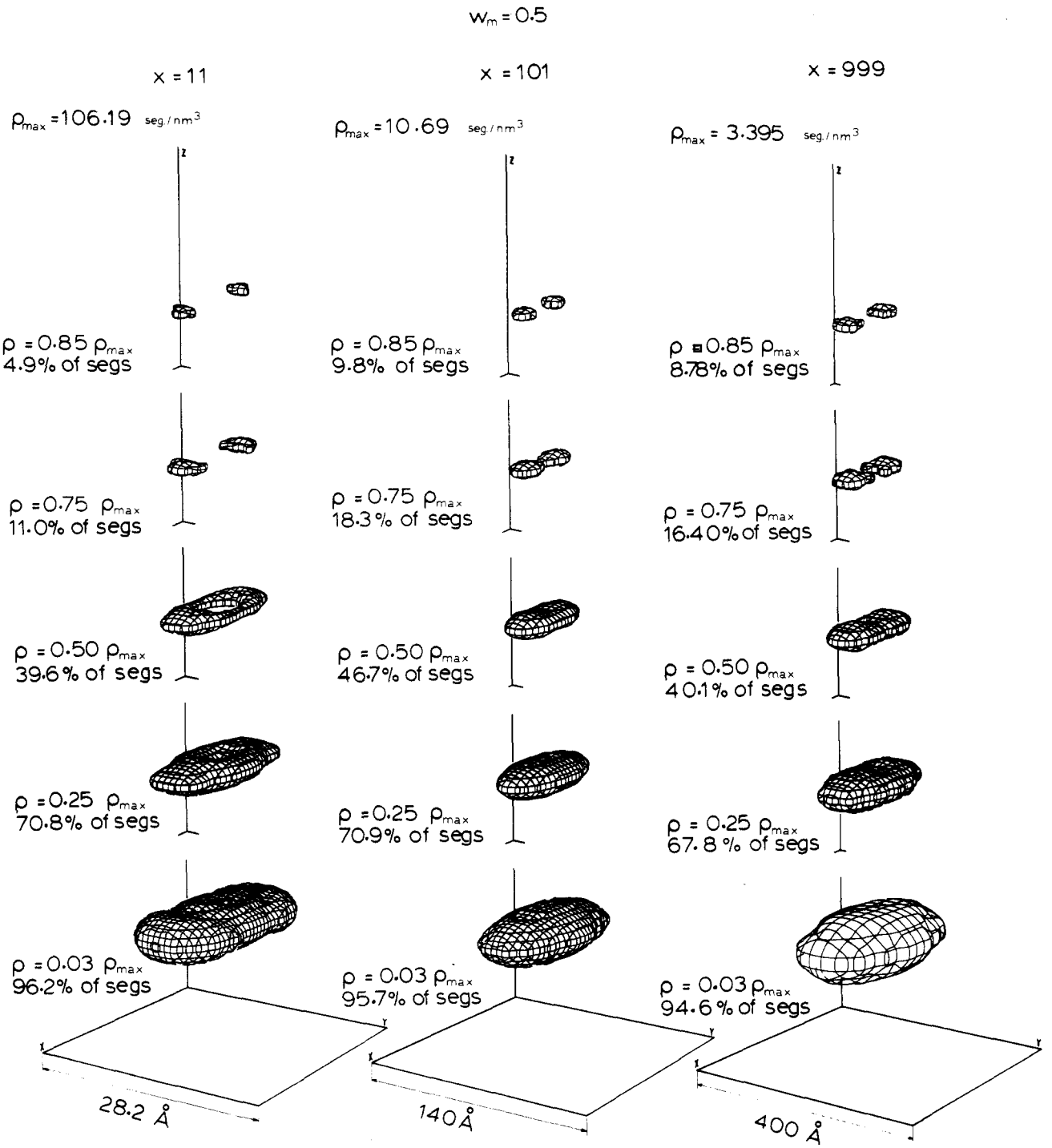

Figure 6. Surfaces of equal average segment density for atactic chains with 50% meso diads of chain length $x = 11$, $x = 101$, and $x = 999$. See legend to Figure 5.

spatial distribution of segments fully confirms the suspicion that a dumbbell-like density distribution characterizes these polymers. The distributions, collected during the Monte Carlo experiments in a 40 × 40 × 40 grid, are visualized here as series of three-dimensional surfaces of constant segment density. Using an established algorithm for drawing isosurfaces[24] we plotted perspective views of closed surfaces that border those regions in space in which the segment density assumes values equal to or higher than a specified limit. The total fraction of segments enclosed by these surfaces is also computed. Figures 5–7 each contain 15 surface plots, for syndiotactic, atactic, and isotactic chains, respectively. Each set of 15 plots contains surfaces for three chain lengths each, i.e., $x = 11$ (short), $x = 101$ (medium), and $x = 999$ (long). For each chain length, in turn, the segment distribution is characterized by five surface plots for segment densities from 3% to 85% of the maximum segment density, ρ_{max}, encountered anywhere in the grid. The actual spatial extent of the closed regions is indicated in the figures.

Directing attention first at the surfaces of low density of the longest chains examined (those surfaces contain essentially all chain segments in the distributions) we observe that Šolc and Stockmayer's[8] early characterization of the segment cloud as a "cake of soap" is remarkably accurate. As we examine the distributions at higher and higher densities, however, striking features become apparent: for all chain lengths and all tacticities examined an indentation, or ridge, develops at the "waistline" of the surfaces; i.e., along the contour in the Y–Z plane, the

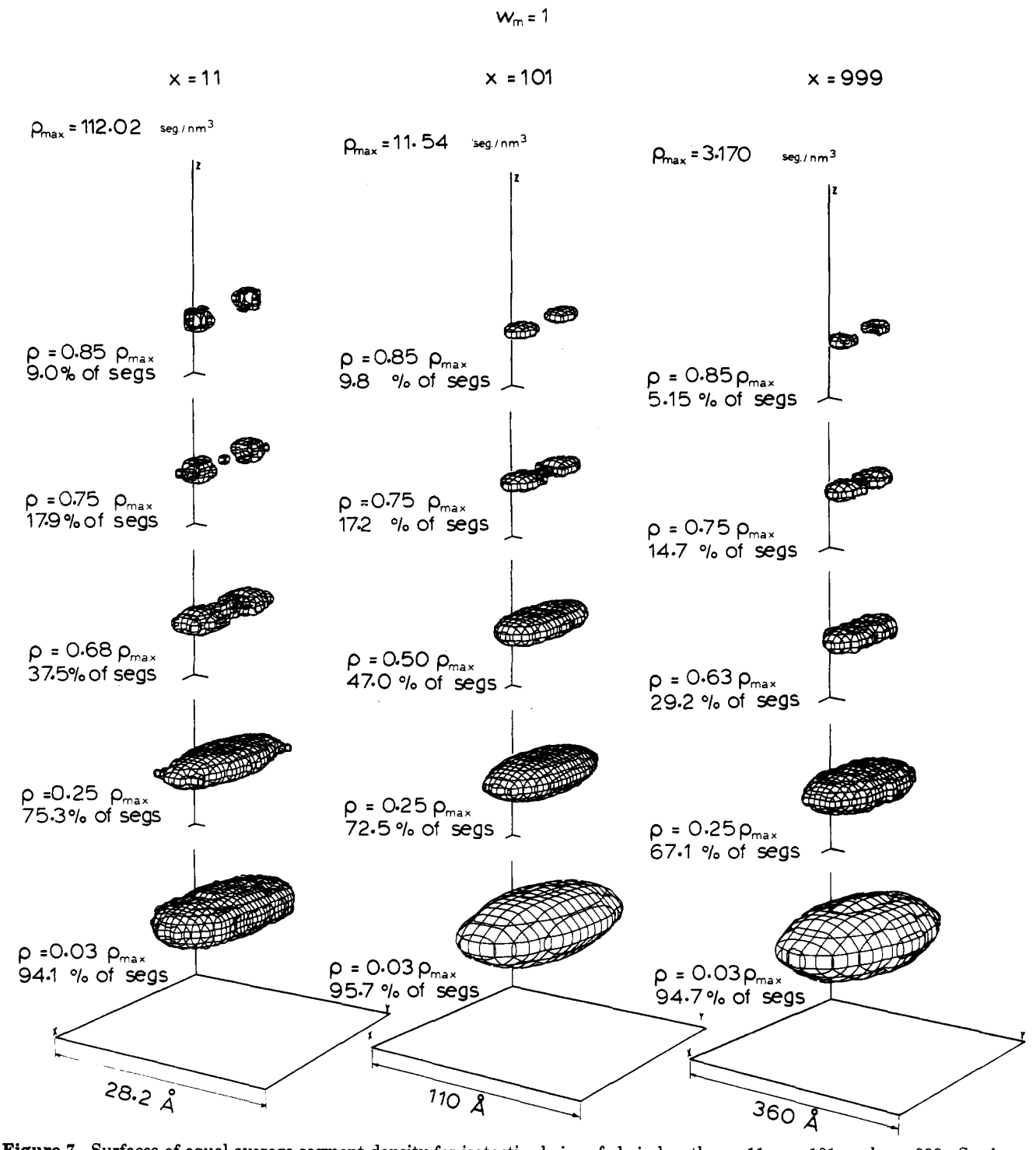

Figure 7. Surfaces of equal average segment density for isotactic chains of chain length $x = 11$, $x = 101$, and $x = 999$. See legend to Figure 5.

distribution becomes bimodal and separates into two distinct domains. The loci of highest density in these dumbbell-shaped distributions are between ca. $1.3\langle s^2\rangle_0^{1/2}$ and $2.0\langle s^2\rangle_0^{1/2}$ apart, the distance being highest for the shortest, and lowest for the longest chains. Short chains, characterized by large ratios between the eigenvalues (see above), assume a characteristic flat and elongated shape.

Chain length and tacticity influence strongly the shapes at intermediate densities, i.e., the way in which the segment distribution separates into two distinct regions. A hole may appear, giving rise to an elongated "doughnut", and subsequently to an arrangement in which the two dense cores are connected by two thin, lateral stems which are ultimately severed, or a single neck may develop and the distribution ultimately break up like a droplet. Even among the longest chains examined there are vestiges of differences due to tacticity in the surfaces at high density.

The maximum segment densities observed in these distributions are consistently higher than those expected at the center of orientationally averaged, spherically symmetric distributions; they are between 15% and 50% above Debye and Bueche's[1,25] estimate for a freely jointed chain with Gaussian segments

$$\rho^{DB}_{max} = (2/n)^{1/2}(9/\pi C_n l^2)^{3/2}, \qquad n \to \infty \qquad (18)$$

If the detailed distributions for the longest chains ($x = 999$) are rotationally averaged a posteriori, however, distributions of essentially Gaussian shape and maximum

densities, very well represented by eq 18, are recovered.

Conclusions

All chains examined, and in our conviction all flexible linear chains, are characterized by bimodal three-dimensional segment density distributions at high segment densities. For all chains the measures of shape indicate a high shape anisotropy for short chain length that decreases within a few hundred skeletal bonds to the limiting values. Long chains at low segment densities resemble a cake of soap, while the detailed shape of short- and medium-length polymers is very dependent on structural details.

Acknowledgment. This work was supported by NSF Grant DMR-8312694 and the Texaco-Manglesdorf Associate Professorship in the Department of Chemical Engineering at MIT. We thank Professors Mattice and Šolc for helpful discussions.

Appendix. Radius of Gyration Tensor and the Reduced Moment of Inertia Tensor

The moment of intertia tensor of a chain, consisting of $n + 1$ "atoms" of equal mass, reduced by the total mass of the chain, is[18]

$$\mathbf{I} = \frac{1}{n+1}\sum_{i=0}^{n}\begin{bmatrix} y^2 + z^2 & -xy & -xz \\ -xy & z^2 + x^2 & -yz \\ -xz & -yz & x^2 + y^2 \end{bmatrix} =$$

$$\mathrm{tr}\,(\mathbf{S})\mathbf{E} - \mathbf{S}$$

where $\mathbf{E}$ is the unit tensor. Hence both $\mathbf{I}$ and $\mathbf{S}$ are diagnoal in the same principal axis system, and in this frame of reference

$$\mathbf{I} = \mathrm{diag}\,(\overline{Y^2} + \overline{Z^2}, \overline{Z^2} + \overline{X^2}, \overline{X^2} + \overline{Y^2})$$

where $\overline{X^2}$, $\overline{Y^2}$, and $\overline{Z^2}$ are the eigenvalues of $\mathbf{S}$, and tr $(\mathbf{I})$ = 2 tr $(\mathbf{S})$.

References and Notes

(1) Debye, P.; Bueche, F. *J. Chem. Phys.* **1952**, *20*, 1337–8.
(2) Flory, P. J. "Principles of Polymer Chemistry"; Cornell University Press: Ithaca, NY, 1953; Chapter XII.2.
(3) Flory, P. J. "Statistical Mechanics of Chain Molecules"; Interscience: New York, 1969; Chapter VIII.
(4) Yamakawa, H. "Modern Theory of Polymer Solutions"; Harper and Row: New York, 1971; Chapter II.7.
(5) Kuhn, W. *Kolloid-Z.* **1934**, *68*, 2–15.
(6) Yoon, D. Y.; Flory, P. J. *J. Chem. Phys.* **1974**, *61*, 5366–80.
(7) Šolc, K. *Polym. News* **1977**, *4*, 67–74.
(8) Šolc, K.; Stockmayer, W. H. *J. Chem. Phys.* **1971**, *54*, 2756–7.
(9) Šolc, K. *J. Chem. Phys.* **1971**, *55*, 335–44.
(10) Koyama, R. *J. Phys. Soc. Jpn.* **1968**, *24*, 580–8.
(11) Mattice, W. *J. Am. Chem. Soc.* **1979**, *101*, 732–6.
(12) Mattice, W. *J. Am. Chem. Soc.* **1979**, *101*, 7651–4.
(13) Mattice, W. *Macromolecules* **1979**, *12*, 944–8.
(14) Mattice, W. *Macromolecules* **1980**, *13*, 904–9.
(15) Mattice, W. *Macromolecules* **1981**, *14*, 863–7.
(16) Rubin, R. J.; Mazur, J. *Macromolecules* **1977**, *10*, 139–49.
(17) The jth invariant of a tensor $\mathbf{A}$, with eigenvalues λ_1, λ_2, and λ_3, is defined as the sum of all subdeterminants of order j, i.e.

$$I_1 = \lambda_1 + \lambda_2 + \lambda_3 = \mathrm{tr}\,(\mathbf{A})$$

$$I_2 = \lambda_1\lambda_2 + \lambda_2\lambda_3 + \lambda_3\lambda_1$$

$$I_3 = \lambda_1\lambda_2\lambda_3 = \det\,(\mathbf{A})$$

(18) Landau, L. D.; Lifshitz, E. M. "Course of Theoretical Physics", 3rd ed.; Pergamon Press: Elmstord, NY, 1976; Volume 1, Chapter VI.
(19) Smith, R. P.; Mortensen, E. M. *J. Chem. Phys.* **1960**, *32*, 502–7.
(20) Flory, P. J. *Macromolecules* **1974**, *7*, 381–92.
(21) Suter, U. W.; Flory, P. J. *Macromolecules* **1975**, *8*, 765–76.
(22) Chapter III.8 of ref 3.
(23) Flory, P. J.; Abe, Y. *J. Chem. Phys.* **1971**, *54*, 1351–63. Also: Nagai, K. *J. Chem. Phys.* **1968**, *48*, 5646–55.
(24) Wright, T. J. *Comput. Graphics* **1979**, *13*, 182–9; subroutine ISOSRF of the SCD Graphics System of the National Center for Atmospheric Research, Boulder, Co.
(25) Reference 4, p 26. Also: Gobush, W.; Šolc, K.; Stockmayer, W. H. *J. Chem. Phys.* **1974**, *60*, 12–21.
(26) Zimm, B. H. *Macromolecules* **1980**, *13*, 592–602.

Uniaxial Draw of Poly(ethylene oxide) by Solid-State Extrusion

Bong Shik Kim and Roger S. Porter*

Polymer Science and Engineering Department, Materials Research Laboratory, University of Massachusetts, Amherst, Massachusetts 01003. *Received October 1, 1984*

ABSTRACT: Ultradrawn filaments of poly(ethylene oxide) (PEO) have been prepared by a solid-state coextrusion in an Instron capillary rheometer. Two different molecular weights, 3.0×10^5 and 4.0×10^6, were evaluated. Properties have been examined as a function of uniaxial draw ratio. The drawn filaments of PEO exhibit extremes of melting point, percent crystallinity, birefringence, and tensile modulus. Features of a PEO filament with a draw ratio of 32 are a 72 °C DSC melting point and a crystallinity of 94.0%, both measured at a scan of 2.5 °C min^{-1}. The corresponding birefringence is 3.5×10^{-2} and the Young's modulus 3.5 GPa.

Introduction

Extrusion of several thermoplastics in the crystalline state has been performed over this past decade.[1,2] A purpose of these studies has been to produce highly oriented morphologies. Despite the great interest in polymer drawing, few studies on poly(ethylene oxide) (PEO) have been reported. Kitao et al.[3,4] employed two different drawing methods: (1) a dry and a wet process each at different temperatures; (2) a melt spinning method. A relatively low draw ratio (7.9), percent crystallinity, and briefringence were reported.

To obtain higher draw ratios and to achieve enhance physical properties, strands of PEO were drawn in this study by solid-state coextrusion by a technique reported by Griswold et al.[5] PEO extrudates of high draw resulting in filaments have been evaluated by thermal analysis, mechanical properties, and birefringence. The method of draw has the advantage of extensional deformation, under pressure and on a substrate for stress distribution.[5-7]

Experimental Section

The samples of PEO used in this study were obtained in powder form from Polyscience, Inc., Pittsburgh, PA. The molecular weights, $\bar{M}_v$, of the poly(ethylene oxide) samples were reported to be 3.0×10^5 and 4.0×10^6. The powders were compression molded for 20 min at 110 °C and 15 000 psi into sheets of 0.2–0.3-mm thickness followed by cooling to ambient. At this stage

0024-9297/85/2218-1214$01.50/0